Available online at www.sciencedirect.com
ScienceDirect
Journal of the European Ceramic Society 28 (2008) 2247–2257
www.elsevier.com/locate/jeurceramsoc

Synthesis and structural characterization of carbon-rich SiC_xO_y derived from a Ni-containing hybrid polymer

Mariana Gava Segatelli [a], Alfredo Tiburcio Nunes Pires [b], Inez Valéria Pagotto Yoshida [a,*]

[a] *Instituto de Química, UNICAMP, 13083-970 Campinas, SP, Brazil*
[b] *Departamento de Química, UFSC, 88040-970 Florianópolis, SC, Brazil*

Received 21 February 2008; accepted 11 March 2008
Available online 2 May 2008

Abstract

Carbon-rich silicon oxycarbide ceramics were obtained by controlled pyrolysis at 950, 1300 and 1500 °C from hybrid polymeric precursors based on poly(methylsiloxane) and divinylbenzene with different molar ratios, in the presence or absence of nickel acetate. By increasing the pyrolysis temperature changes in the local molecular structure were observed by ^{29}Si NMR, with the segregation of thermodynamically stable SiO_2 and SiC phases, in addition to formation of graphitic carbon nanoclusters. Ceramics without Ni were amorphous at 950 °C, while those obtained at 1300 °C showed the presence of a β-SiC phase. The presence of Ni in the polymeric precursor induced the formation of β-SiC, cristobalite silica, graphitic carbon, metallic Ni, NiO and Ni_2Si, and also reflected in denser materials. In general, the resulting ceramics without Ni did not present measurable porosity, whereas Ni-containing ceramics at 1500 °C showed behavior typical of mesoporous materials.

Keywords: Polymer pyrolysis; SiC; Carbides; Glass ceramics

1. Introduction

In recent decades, polymer-derived ceramics (PDCs) obtained via pyrolysis of Si-containing polymers, such as polysiloxanes, have been a principal focus of many studies for silicon oxycarbide (SiC_xO_y) production.[1–10] The attractive properties of SiC_xO_y glasses, such as materials for high temperature applications or electronic packaging, associated to the possibility to process the final products using relatively easy polymer processing techniques, make PDC a suitable route to tailor these glasses.[11] It is well-established that the organic–inorganic transition in the pyrolysis of polysiloxanes occurs between 600 and 800 °C, resulting in a SiC_xO_y metastable amorphous phase characterized by a random distribution of different Si sites, in addition to carbon dispersed phase. At temperatures of ∼1000 °C, an extended SiC environment can be observed in some SiC_xO_y glasses, particularly when polymeric precursors rich in Si–C bonds are used, which allow a local arrangement close to that found in crystalline SiC.[4–11] Higher temperatures, usually greater than 1200 °C, initiate the crystallization of thermodynamically favorable phases such as β-SiC, cristobalite silica (c-SiO_2) and also a C-graphitic phase.[12,13] It is important to emphasize that most SiC_xO_y glasses are obtained from precursors prepared by hydrolysis/condensation routes, which give rise to glasses with higher O/Si molar ratios.[3,7,11,13]

The polymeric precursor parameters, such as chemical composition and network architecture, associated with the residual porosity of the resulting ceramic phase, usually affect the crystallization behavior of the amorphous ceramic matrix.[12] In addition, the increase in the number of elemental constituents in the ceramic matrix contributes to improve thermal stability against crystallization.[14–17]

Kleebe et al.[11] described the microstructural evolution of a stoichiometric SiCO material using high resolution transmission electron microscopy (HRTEM) and electron energy-loss spectroscopy (EELS) analysis. The phase separation in this system starts at about 1200 °C and results in the formation of a nanosized SiC precipitate embedded in amorphous SiO_2, which is dispersed in a SiCO environment. The crystallization process is nearly complete in the material obtained at ∼1400 °C. HRTEM and EELS were similarly used to investigate the densification/crystallization behavior of two SiC_xO_y ceramics obtained

* Corresponding author. Tel.: +55 19 3521 3130; fax: +55 19 3521 3023.
E-mail address: valeria@iqm.unicamp.br (I.V.P. Yoshida).

0955-2219/$ – see front matter © 2008 Elsevier Ltd. All rights reserved.
doi:10.1016/j.jeurceramsoc.2008.03.001

from different polymeric precursors.[13] The densification and crystallization behavior were shown to be dependent on their corresponding starting compositions.

More recently, the use of some transition metals for the production of structures on the micrometric/nanometric scale, such as tubes, wires and rods, has been described.[18–20] Among the selected metals, nickel has received a special attention due to its catalytic activity in promoting the nucleation of such structures.[21] In these studies, the main interest was focused on evaluation of different growth mechanisms of these nanostructures using several morphological characterization techniques. However, the structural evolution of nickel-containing PDC has not been explored very well.[18]

The present study focuses on the preparation of carbon-rich silicon oxycarbide (SiC_xO_y) having differing carbon amounts from the pyrolysis of hybrid polymeric precursors derived from poly(methylsiloxane) (PMS) and divinylbenzene (DVB) in different molar ratios, in the presence or absence of anhydrous nickel acetate (NiAc). The thermal and structural characterization of the materials starting from polymer and leading to ceramics is discussed. The effect of adding NiAc to the polymeric precursors on the final characteristics of the Ni-containing ceramics was investigated.

2. Experimental procedure

2.1. Starting materials

Poly(methylsiloxane), $(HSi(CH_3)O)_n$, PMS, with a molar mass of ~2000 g/mol (Dow Corning, Hortolândia, Brazil) and divinylbenzene (DVB) (Aldrich, Milwaukee, USA) were used to produce PMS/DVB hybrid polymeric networks by the hydrosilylation reaction catalysed by 1,3-divinyl-1,1,3,3-tetramethyldisiloxane platinum complex (Pt catalyst, 3–3.5% platinum concentration in vinyl-terminated poly(dimethylsiloxane)), from Gelest (ABCR GmbH., Karlsruhe, Germany). Nickel acetate tetrahydrate (Vetec Química Fina Ltda, Rio de Janeiro, Brazil), was previously dried (NiAc), and toluene P.A. (Synth, Diadema, Brazil) was employed as solvent for the hydrosilylation reaction.

2.2. Synthesis of the hybrid polymeric precursors and pyrolysis

The PMS/DVB hybrid polymeric precursors were obtained by the hydrosilylation reaction between PMS and DVB, resulting in crosslinked networks, using a procedure similar to that previously described.[22] The PMS/DVB hybrid polymers were prepared in 70/30, 50/50 and 30/70 ratios, in relation to the Si–H: C=C molar ratio, as described in Table 1, in order to generate polymeric networks with different amounts of aromatic carbon bridges.

DVB was first mixed with the Pt-catalyst (~10 ppm relative to PMS mass). The solution was maintained at 0 °C, under an argon atmosphere and PMS was slowly added. The temperature was allowed to reach 25 °C and the resulting solution was stirred for ~20 min, until a visible increase of its viscosity. The viscous solution was cast into Teflon molds of 13.5 cm × 1.3 cm × 0.3 cm and the final products were cured for 48 h at room temperature. Additional curing was then carried out at 100 °C in a vacuum oven for 8 h. The NiAc-containing hybrid polymeric precursors were prepared by the same procedure, with the addition of 3 wt% NiAc dispersed in toluene to the reaction solution. The cured hybrid polymeric networks, with and without NiAc, were heated at 250, 450, 700 and 950 °C, using a heating rate of 5 °C/min and a holding time of 30 min at the selected final temperature, excepted for 950 °C (holding time of 60 min). The pyrolyses were carried out in an EDG 5P tubular furnace, equipped with an internal alumina tube and a temperature controller, under flowing argon (100 mL/min). For samples obtained at 1300 and 1500 °C, the pyrolysis process was carried out from samples previously pyrolysed at 950 °C, with a holding time of 60 min at the final temperature, in a Thermolyne F59340-CM tubular furnace.

Table 1
Composition of PMS/DVB hybrid polymers with and without NiAc, in relation to the Si–H: C=C molar ratio

Hybrid polymers	70/30	50/50	30/70
PMS/DVB	H1	H2	H3
PMS/DVB + NiAc	HNi1	HNi2	HNi3

2.3. Characterization techniques

The ceramic yield and the thermal stability of the hybrid polymers were evaluated by thermogravimetry (TG), using a thermobalance (2950 TA Instruments) in the temperature range of 25–950 °C, at a scanning rate of 20 °C/min, under flowing argon (100 mL/min). The structural evolution from the hybrid polymeric network to SiC_xO_y ceramic was monitored by infrared (IR) spectroscopy, using the conventional KBr pellet technique and a Bomen B100 spectrometer, operating in the transmission mode between 4000 and 400 cm^{-1}, at 4 cm^{-1} resolution. X-ray diffraction (XRD) patterns were recorded on a Shimadzu diffractometer model XRD6000 operating at 40 kV and 30 mA, with Cu Kα radiation (λ = 1.54060 Å). The estimated average crystal size was determined according to the Scherrer equation.[23,24] Density measurements were performed in a helium pycnometer (Micromeritics, model 1305), using helium as carrier gas. The analyses were conducted with samples dried at 120 °C for 1 h and purged with He at least 10 times before measuring. These measurements correspond to absolute density and, in this study, they will be referred to only as density. NMR spectra were recorded on a spectrometer (Bruker Avance II-400) operating at 79.46 and 100.58 MHz for ^{29}Si and ^{13}C nuclei, respectively, applying the magic angle spinning (MAS 54.74°) technique. The analyses were acquired employing the HPDEC (High Power Decoupling) method. The recycle delay used for ^{29}Si one-pulse experiments was 300 s with a 90° flip angle and acquisition time of 25 ms. ^{13}C NMR spectra were registered with a recycle delay of 60 s and acquisition time of 34 ms. In ^{29}Si NMR experiments, the compound used as chemical shift refer-

ence was kaolin (−91.2 ppm in relation to tetramethylsilane), and in the ^{13}C NMR, adamantane (38.3 ppm from tetramethylsilane). Micro-Raman spectroscopy measurements were performed using a Renishaw Raman microscope. Laser light at 514.5 nm from an Ar laser was used for excitation. A potency of 1.1 mW cm^{-2} was employed and calibration was carried out with the Si peak at 520.7 cm^{-1}. The error in the peak positions was less than ±2.0 cm^{-1}. Carbon elemental analyses were performed in an elemental analyzer (PerkinElmer 2400 Series II) using the procedure suggested in Ref. [25]. The Si content in the ceramic products was evaluated by X-ray micro-fluorescence (μEDX), in an X-ray micro-fluorescence spectrometer (Shimadzu 1300). The oxygen content was estimated by difference. The specific surface area and pore size distribution analyses were carried out from nitrogen adsorption experiments by means of the physical adsorption method, using an automatic nitrogen gas adsorption instrument (ASAP 2010, Micromeritics) and standard procedures described in literature.[26] From the isotherms, specific surface area and pore volume, together with pore size distribution, were obtained. The specific surface area was determined from adsorption isotherms using the Brunauer, Emmett and Teller (BET) method.[27] The pore size distribution was obtained from the desorption isotherm, according to Barret, Joyner and Halenda (BJH) method,[28] assuming that all pores are cylindrical and closed at one end.

3. Results and discussion

3.1. Synthesis and curing of the polymeric precursors

The hydrosilylation reaction between PMS and DVB, catalysed by the Pt (II) complex, was based on an addition reaction involving the Si–H and C=C bonds, where no by-product was generated. The formulations were converted overnight at room temperature into resinous materials. To guarantee the maximum level of crosslinking, the hybrid polymers were submitted to a post-curing process, as described in the experimental section. The resulting polymers showed densities of 1.1 g/cm^3, characteristic of polymeric material. The transparency and brittleness of these polymers were reduced with increases of the initial amount of DVB. This effect is probably associated with radical polymerization reactions between the residual vinyl groups from DVB, which contribute to the shrinkage and the micro-cracks observed in the PMS/DVB 30/70 polymers. The NiAc-containing materials showed a green color, which is characteristic of Ni^{2+}, as expected. In the prepared hybrid polymeric networks, the bridges between two siloxane chains were mainly constituted by 1,4-diethylphenylene, as can be seen in Fig. 1. The PMS/DVB hybrid polymer obtained from 70/30 molar ratio showed an excess of Si–H bonds after the post-curing step, which can contribute to de-hydrogen coupling parallel reactions. During the curing step, performed in air at room temperature, the Pt-catalyst also promotes the reaction between the residual Si–H bonds and environment moisture, giving rise to Si–OH groups that, in subsequent steps, produce Si–O–Si bridges between siloxane chains. Considering that both PMS and DVB were incorporated in the polymeric network, the initial C/Si compositions of PMS/DVB 70/30, 50/50 and 30/70, taking into account the Si–H: C=C molar ratio, were 5.3, 12.3 and 28.7, respectively.

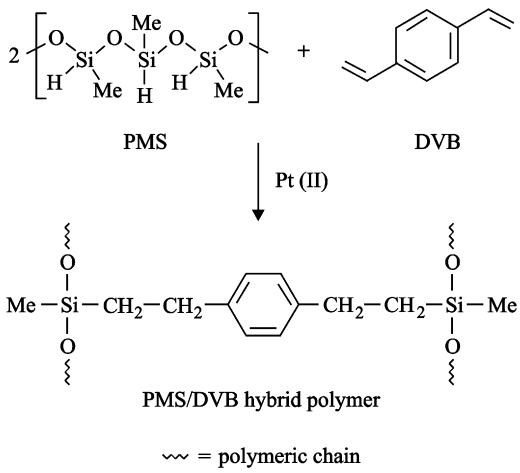

Fig. 1. Reaction between PMS and DVB giving rise to PMS/DVB hybrid polymer.

3.2. Thermal stability of the polymeric precursors

The thermal behaviors for PMS/DVB hybrid polymers (H1, H2 and H3) are shown in Fig. 2. These polymers presented good thermal stabilities, with initial weight loss temperatures at 452, 433 and 428 °C, respectively. Two weight loss steps were observed in the ranges: 452–644 °C and 644–786 °C for H1, corresponding to a weight loss of 12.10 and 3.70%, respectively; 433–631 °C and 631–777 °C for H2 (weight loss of 23.19 and 2.82%, respectively) and 428–626 °C and 626–783 °C for H3 (weight loss of 25.28 and 4.37%, respectively). These degradation steps can be clearly seen in Fig. 2b. It is well established that the initial thermal decomposition process of polysiloxanes occurs by inter and/or intrachain rearrangements, generating volatile cyclic structures.[6,29,30] However, these volatiles structures are generally formed when the polymer or the network is constituted by long chains and/or reactive end groups, as Si–OH. This behavior is not expected in the hybrid polymeric networks studied. Thus, up to ∼460 °C, the weight loss was related to the degradation of organic groups, mainly CH_3 and CH_2–CH_2. From 500 to 800 °C, part of the phenyl rings can be degraded, followed by the mineralization of the PMS/DVB residual material.[31] In this last step, redistribution reactions involving different silicon sites can also take place, giving rise to silicon oxycarbide.

The ceramic yields of PMS/DVB in 70/30, 50/50 and 30/70 molar ratios were 83, 72 and 69%, respectively. These ceramic yields were associated to the crosslinking degree of the hybrid polymeric network and were also inversely related to the organic amount (DVB) in the material.[22,32] Thus, the results for the ceramic yield were in agreement with the chemical compositions of the polymeric precursors.

The NiAc-containing PMS/DVB hybrid polymers (HNi1, HNi2 and HNi3) showed similar thermal behavior to those polymers without NiAc (not shown), except for the appearance of

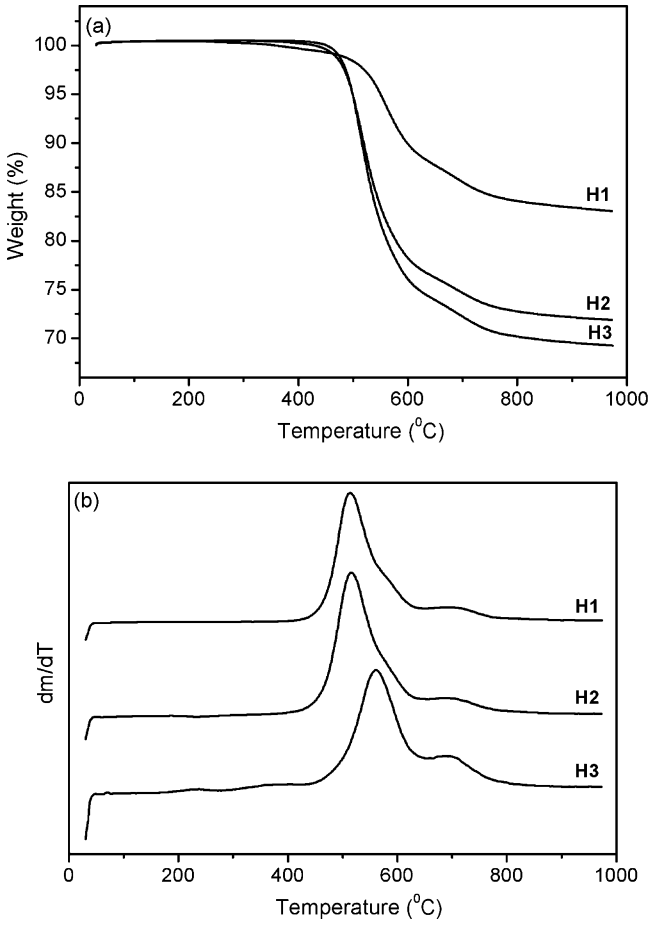

Fig. 2. TG (a) and DTG (b) curves for the PMS/DVB hybrid polymers at 70/30 (H1), 50/50 (H2) and 30/70 (H3) molar ratios.

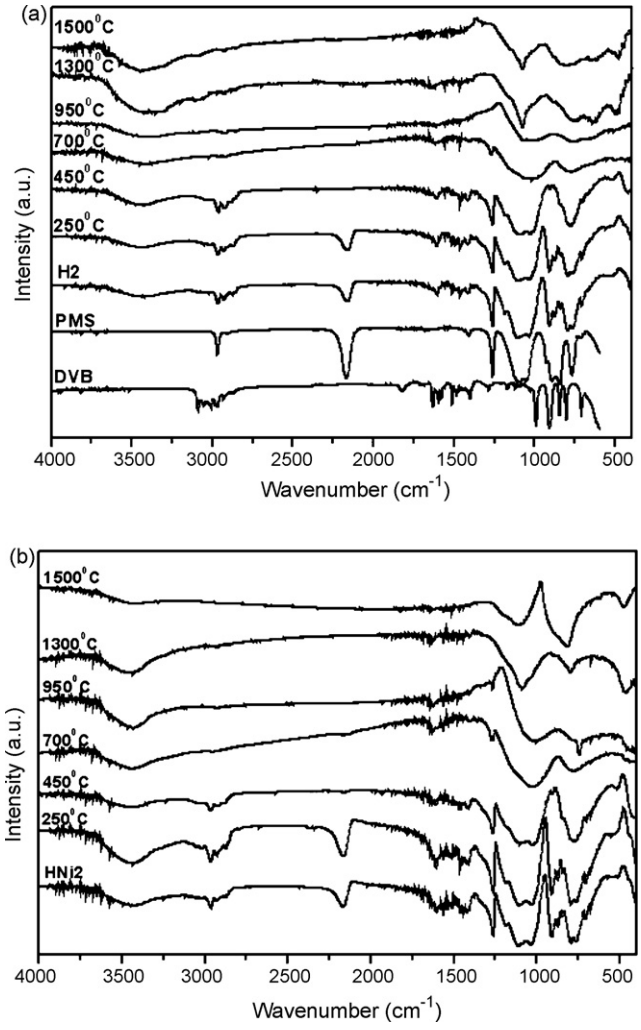

Fig. 3. IR spectra of DVB, PMS, the H2 ceramic (a) and the HNi2 ceramic (b) heated at different temperatures.

the first decomposition step, corresponding to acetate degradation from NiAc. In this way, these hybrid polymers revealed practically the same values of ceramic yields (82, 73 and 69%), indicating that the addition of the NiAc to the polymeric precursor did not change the thermal degradation mechanism of the hybrid polymeric networks.

3.3. Elemental and structural characterization of SiC_xO_y-based ceramics

The structural evolution from PMS/DVB hybrid polymers to ceramic material, as a function of the heat treatment, was monitored by IR spectra, as illustrated for H2 (Fig. 3a) and HNi2 ceramics (Fig. 3b). The PMS and DVB spectra are also shown for comparison. For both samples, a drastic reduction in the relative intensity of νC–H (C=C) (3055 cm^{-1}) and νSi–H (2160 cm^{-1}) absorptions[33] was observed, when compared to the DVB and PMS spectra. These results indicate that the hydrosilylation reaction between PMS and DVB was effective, generating the H2 and HNi2 precursors with low quantities of residual functional groups, which could be detected as very weak absorptions up to 450 °C, in addition to those related to the siloxane chains. For samples heated at 700 °C, the mineralization process was practically complete. The H2 sample heated at 950 °C showed two broad bands at 1080 and 800 cm^{-1}, assigned mainly to νSi–O–Si and νSi–C absorptions, respectively, as expected for this ceramic material. However, in the ceramics obtained at 1300 °C and 1500 °C, a reduction of the relative intensity and width of the absorption centered at 1080 cm^{-1} (νSi–O–Si) was verified. The absorption corresponding to the νSi–C did not present a significant change in intensity and width. It is well known that SiC is formed at temperatures higher than 1300 °C by a carbothermal reduction reaction of Si–O-rich sites present in an amorphous SiC_xO_y phase.[10,16] The weak absorption at 480 cm^{-1}, characteristic of νSi–O, corresponds to the mode associated with cyclic siloxane.

Ni-containing materials (HNi2) obtained up to 700 °C showed similar spectra, in relation to the corresponding samples derived from H2. From 950 to 1500 °C, a considerable reduction in the intensity of the absorption corresponding to νSi–O–Si and a pronounced increase of the relative intensity of the band at 800 cm^{-1}, assigned mainly to νSi–C, were observed. This result suggests that the presence of Ni induced the formation of a SiC crystalline phase, with the consumption of Si–O-rich sites.

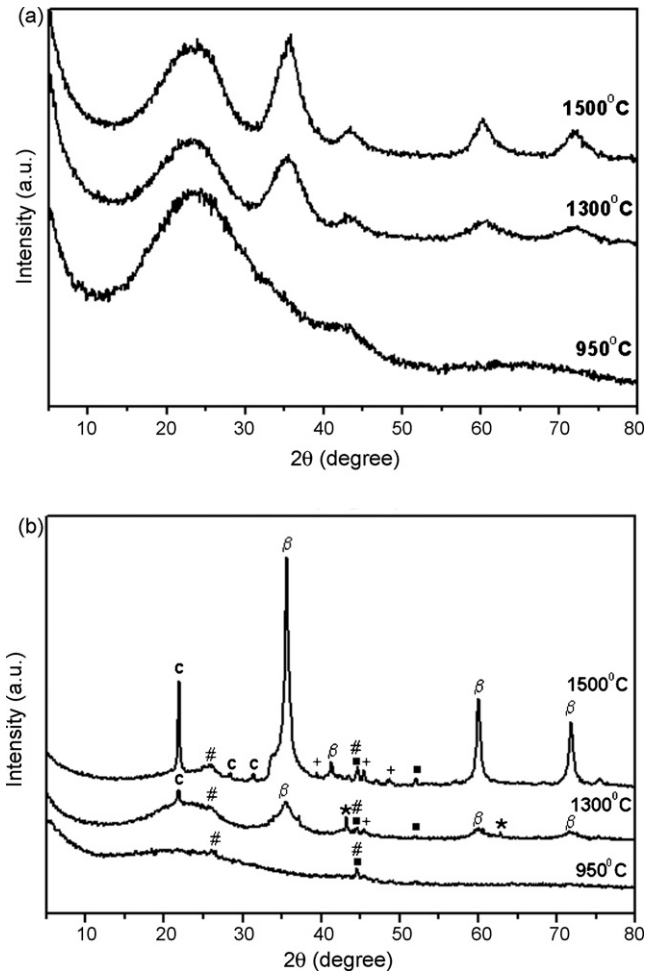

Fig. 4. XRD patterns of the H2 ceramic (a) and the HNi2 ceramic (b) heated at different temperatures, where c is cristobalite; β, β-SiC; (■) Ni; (*) NiO; (+) Ni_2Si and (#) C-graphitic.

XRD patterns of the H2 and HNi2 ceramics pyrolysed at different temperatures are reported in Fig. 4a and b, respectively. H2 obtained at 950 °C showed a broad halo centered at about 24° (2θ), typical of amorphous SiC_xO_y.[10] The increase of the pyrolysis temperature to 1300 and 1500 °C promoted the crystallization of a β-SiC phase, characterized by broad diffraction peaks at 35.5°, 43°, 60° and 72° (2θ), corresponding to (1 1 1), (2 0 0), (2 2 0) and (3 1 1) SiC planes, respectively.[34,35] In addition to these peaks a broader halo centered at 22° (2θ), assigned to opaline silica,[36,37] was also observed. On the other hand, the presence of Ni metal allowed a more effective crystallization in the corresponding ceramic, HNi2, mainly at 1500 °C, as can be seen in Fig. 4b. Sharp and well defined peaks from the β-SiC phase, together with the characteristic diffractions of crystalline cristobalite silica at 22°, 28.5° and 31.5° (2θ)[38] and also two less intense peaks at 26.1° and 44.3° (2θ), attributed to the corresponding (0 0 2) and (1 0 0) graphitic carbon planes,[21,39] were verified. The less intense peaks at 43.3° and 62.9° (2θ) correspond to (2 0 0) and (2 2 0) of the NiO planes,[40] respectively, while the peaks at 44.5° and 52.0° (2θ) are characteristics of metallic nickel, corresponding to its (1 1 1) and (2 0 0) planes, respectively.[21] In addition, diffraction peaks at 39°, 45.4° and 49° (2θ), attributed to a Ni_2Si phase, were also observed in the ceramic specimens obtained at 1300 and 1500 °C.[18] Similar crystalline behavior was observed for the ceramics prepared from other compositions.

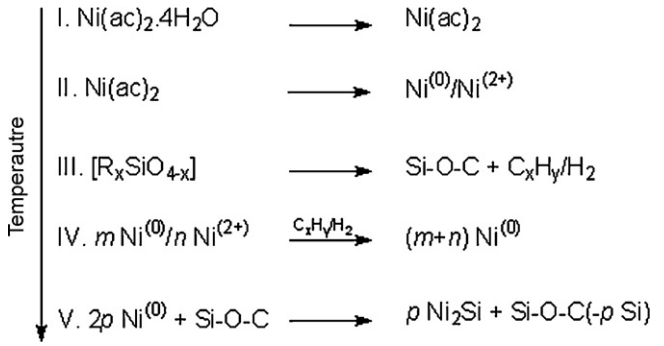

Fig. 5. Proposed reactions for the formation of the Ni and Ni_2Si catalytic particles in the polymer-derived-ceramic during heating and pyrolysis in an Ar atmosphere.[18] The temperature increases from I to V.

The formation of Ni and Ni_2Si particles can be explained by oxi-reduction reactions that occur concomitant to the degradation of the PMS/DVB network, in the similar way to that described by Scheffler et al.[18] in polysilsesquioxane pyrolysis. Fig. 5 shows reaction pathways for the formation of these particles. In the first step, from 90 to 150 °C, $Ni(Ac)_2{\cdot}4H_2O$ dehydrates, giving rise to anhydrous $Ni(Ac)_2$. With increasing temperature, this latter degrades with the formation of Ni^0 and Ni^{2+} species, according to step II. Following, the remaining Ni^{2+} species can easily be reduced by hydrogen and hydrocarbon action, produced by thermal decomposition of the polymeric precursors (steps III and IV). Finally, Ni_2Si particles are formed between 1300 and 1500 °C, according to step V.

The effect promoted by the pyrolysis temperature and the presence of Ni^0 and/or Ni_2Si particles on the crystallization of the ceramics resulted in larger SiC nanocrystals and consequent changes in the density of the materials. It is well known that SiC_xO_y glasses derived from polymeric precursors present a glass transition temperature in the 1300–1350 °C range.[41,42] Thus, a viscous sintering process above the glass transition temperature of the SiC_xO_y glass is responsible for the densification process of the pyrolysed specimens. In addition, the carbothermal reduction reaction also contributes to the formation of the β-SiC crystalline phase (density of 3.2 g/cm^3)[43] and, consequently, to the increase of the density value. Table 2 shows the estimated average size of the β-SiC crystals and density values of the resulting ceramics with and without Ni at different pyrolysis temperatures. For both sets of sample, the density was 1.1 g/cm^3 up to 450 °C, typical of the polymeric material. The density of the ceramics increases with the increase of the pyrolysis temperature, in the 700–1500 °C range, which is associated with the mineralization and, after this, to the crystallization processes. The ceramic materials obtained with Ni showed a tendency to be denser than similar ones without Ni. This fact is related to the higher crystallinity of the former with higher average β-SiC sizes, particularly the HNi3 sample obtained at 1500 °C, which showed the highest density value and an average β-SiC crystal size of 42.8 nm, in addition to the presence of other minor-

Table 2
Average size of the β-SiC crystals and density values for the ceramic specimens with and without Ni at different pyrolysis temperatures

	Samples	Average β-SiC crystal size (nm)[a]		Density (g/cm^3)			
		1300 °C	1500 °C	700 °C	950 °C	1300 °C	1500 °C
Without Ni	H1	5.9	5.9	1.4 ± 0.002	1.7 ± 0.001	1.9 ± 0.003	1.9 ± 0.002
	H2	4.7	5.1	1.3 ± 0.001	1.6 ± 0.003	1.8 ± 0.002	1.8 ± 0.003
	H3	4.8	5.0	1.3 ± 0.002	1.6 ± 0.001	1.7 ± 0.002	1.7 ± 0.002
With Ni	HNi1	6.2	19.8	1.5 ± 0.003	1.8 ± 0.003	2.0 ± 0.002	2.2 ± 0.002
	HNi2	6.9	24.2	1.4 ± 0.002	1.6 ± 0.001	1.5 ± 0.002	1.9 ± 0.003
	HNi3	17.4	42.8	1.5 ± 0.003	1.7 ± 0.002	1.9 ± 0.001	2.5 ± 0.003

[a] Values estimated by Scherrer equation[23,24] using the diffraction peak at 35.5° (2θ).

ity crystalline phases. These results are in complete agreement with data reported in the literature for SiC_xO_y-based materials containing heteroatoms.[15–17]

Table 3 illustrates the elemental composition data for the ceramic samples, with and without Ni, obtained at 950 and 1500 °C. Scheffler et al.[18] revealed that the oxygen content for Ni-free samples derived from poly(methylphenylsilsesquioxane) was higher from 700 to 1000 °C, while the Ni-loaded samples exhibited a significantly higher carbon content. The carbon content in all samples obtained at 950 °C, expressed in the empirical formula, is in agreement with the DVB amount incorporated in the polymeric network. In general, the carbon and oxygen contents for ceramics without Ni showed a tendency to increase with increasing pyrolysis temperatures, while the Ni-containing ceramics showed a reduction in the carbon amount with the increase of the pyrolysis temperatures. The oxygen content for the investigated compositions, independent of the pyrolysis temperature, was higher for the corresponding Ni-containing ceramics. In addition, the increase in the pyrolysis temperature led, in general, to a high segregation of the carbon phase resulting in higher C_{free} amounts. The ceramics without Ni presented higher C_{free} amounts than the respective Ni-containing ceramics.

The evolution of the molecular structure during the pyrolysis, in relation to the local silicon environments, monitored by ^{29}Si MAS NMR spectra, was similar for all studied compositions, as illustrated for H1 and HNi1 in Fig. 6. The samples obtained at 950 °C showed typical profiles of SiCO disordered networks with broad peaks associated with different Si-units.[9] Five signals could be identified in the H1 and HNi1 samples at about −106, −71, −33, −14 and −6 ppm, which were attributed to SiO_4 (Q), SiO_3C (T), SiO_2C_2 (D), SiC_4 (C) and $SiOC_3$ (M) units,[2,4,6] respectively. According to the spectra, the relative amount of these species is strongly dependent on the pyrolysis temperature and less dependent on Ni addition in the polymeric network, as can be seen in Table 3. At higher pyrolysis temperatures, the amount of SiO_4 and SiC_4 units significantly increased, resulting in the formation of Si–O-rich and Si–C-rich domains due to redistribution reactions around the Si atoms, giving rise to a continuous phase separation process, which, at 1500 °C, is characterized by SiO_4 and SiC_4 environments associated to the thermodynamically stable SiO_2 and SiC phases, respectively. The relative intensities of the SiO_4/SiC_4 ratios were 0.83 and 0.44 for H1 and HNi1 samples obtained at 1500 °C, indicating that, in the latter, there is a relatively higher amount of SiC phase inserted in the ceramic matrix, in agreement with IR and XRD data. The other formulations (H2, H3, HNi2 and HNi3) showed similar profiles, stressing the inductor effect of Ni on the crystallization behavior, and consequently, on the phase separation in these systems.

The carbon phase dispersed in the ceramic matrix was evaluated by ^{13}C MAS NMR spectra, which provided information

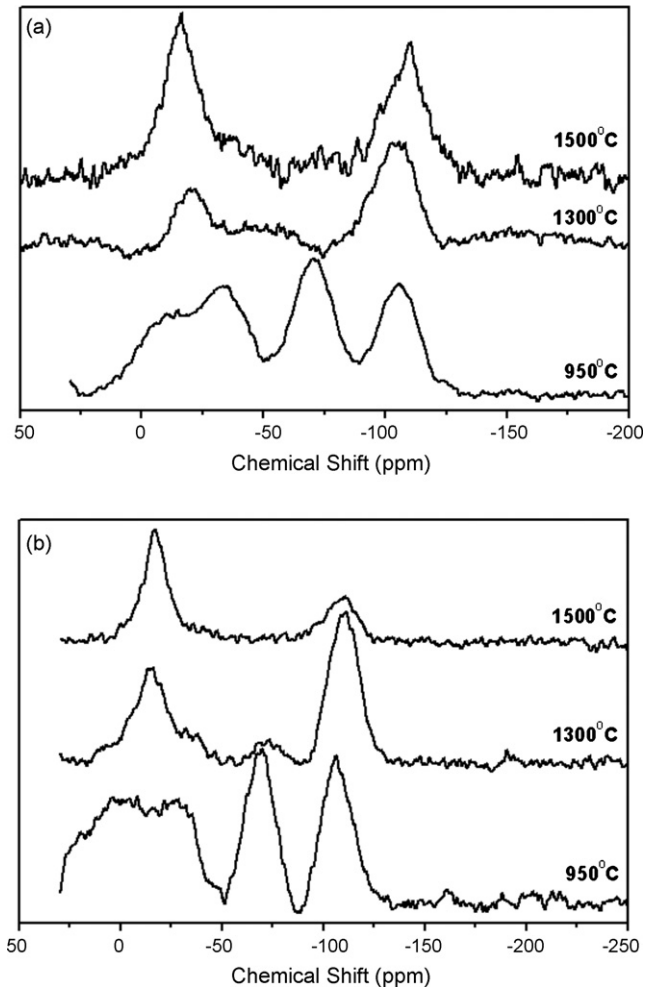

Fig. 6. ^{29}Si MAS NMR spectra for the H1 (a) and HNi1 (b) ceramic samples obtained at different pyrolysis temperatures.

Table 3
Elemental composition of the ceramic specimens with and without Ni obtained by pyrolysis, in an argon atmosphere, at 950 °C and 1500 °C, and distribution of silicon sites (obtained from ^{29}Si MAS NMR spectrum)

Samples/temperature (°C)	Elemental analysis	NMR MAS ^{29}Si Silicon sites (%)					C_{free} (%)
	Empirical formula[a]	Q	T	D	M	C	
H1/950	$SiC_{2.02}O_{0.66}$	23.60	29.71	27.05	15.27	4.37	51.77
H1/1500	$SiC_{2.13}O_{0.81}$	39.10	11.15	7.87	–	41.87	51.41
H2/950	$SiC_{2.59}O_{0.66}$	27.54	19.70	5.13	–	47.62	44.89
H2/1500	$SiC_{2.64}O_{0.73}$	52.33	4.26	–	–	43.41	55.52
H3/950	$SiC_{3.06}O_{0.86}$	29.33	19.94	6.89	–	43.84	47.73
H3/1500	$SiC_{3.33}O_{0.73}$	40.07	12.55	–	–	47.37	49.49
HNi1/950	$SiC_{2.30}O_{1.13}$	22.41	21.50	7.58	28.55	19.95	28.06
HNi1/1500	$SiC_{1.98}O_{1.25}$	40.98	–	–	–	59.02	40.98
HNi2/950	$SiC_{2.62}O_{0.79}$	21.63	20.05	5.28	–	53.04	39.31
HNi2/1500	$SiC_{2.57}O_{0.89}$	52.77	3.22	–	–	44.02	55.17
HNi3/950	$SiC_{3.37}O_{1.24}$	29.88	18.26	6.43	–	45.42	46.80
HNi3/1500	$SiC_{2.28}O_{0.63}$	37.59	–	–	–	62.41	37.59

[a]Empirical formula normalized to one Si atom.

about the local environments of carbon sites in the ceramic samples. The behaviors observed for the compositions studied are similar to those illustrated for the H1 and HNi1 samples in Fig. 7. These samples also showed similar profiles indicating that the presence of Ni did not promote significant disturbances in the C-environments of these ceramics, to be detected by this technique. The free carbon amount is associated with the incomplete decomposition of organic segments, such as methyl and phenyl groups present in the polymeric network.[44] Three main signals can be seen in the samples obtained at 950 °C: the resonance around +25 ppm is assigned to aliphatic carbon (Csp^3 sites); the relatively strong and broad resonance centered around +124 ppm confirms the presence of a relatively high amount of aromatic carbon (Csp^2 sites)[44] and the signal centered at +136 ppm is associated to graphitic carbon. These last two Csp^2 sites represent the formation of a separate "free carbon" phase (individual carbon clusters and graphitic carbon).[9] The increase of the pyrolysis temperature led to a reduction of the aliphatic carbon signal and an increase in Csp^2 sites, as expected, where the graphitic carbon signal was less pronounced, although the XRD patterns showed an opposite behavior. This apparent discrepancy can be understood by the relatively low C-graphitic signal in the ceramic samples and also to the difficulty to obtain a quantitative ^{13}C MAS NMR analysis of these samples due to the higher recycle delay necessary to determine the amounts, particularly with the increase of the sizes of the graphitic carbon. The experimental ^{13}C NMR parameters are essential to define appropriate signals and, in this case, the samples should be evaluated under different experimental conditions. However, this evaluation was not possible due to time limitations. However, the present data indicate that the interpretation of this analysis must be done very carefully.

Raman spectroscopy is an efficient tool for the evaluation of C-containing materials and, in this study, it was employed to acquire information about structural evolution, in particular, of the free carbon phase dispersed in the SiC_xO_y matrix obtained at different pyrolysis temperatures.

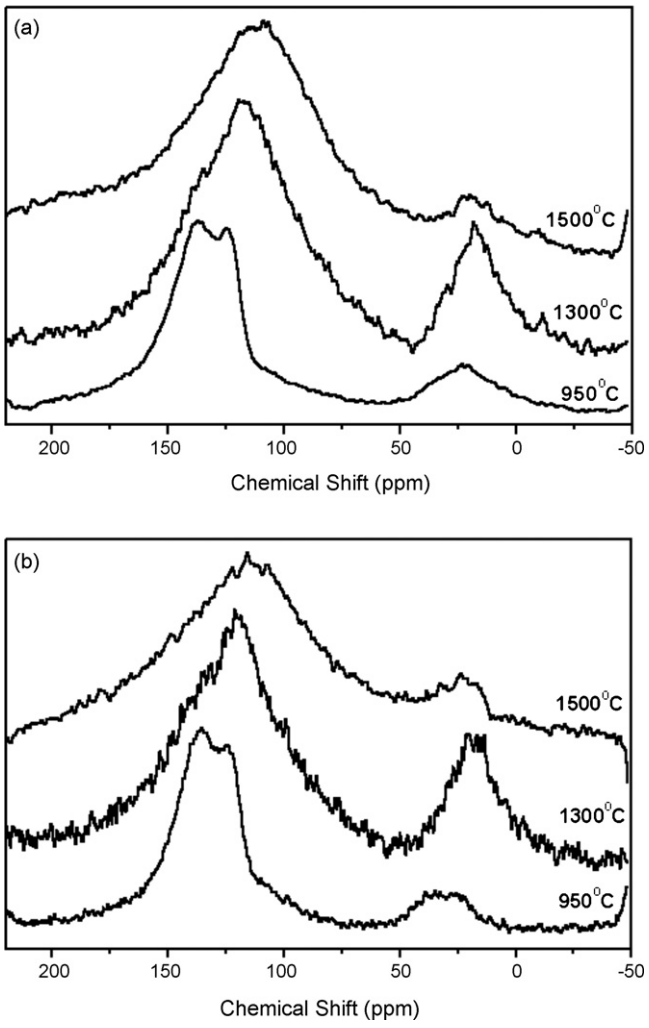

Fig. 7. ^{13}C MAS NMR spectra for the H1 (a) and HNi1 (b) ceramic samples obtained at different pyrolysis temperatures.

The first-order Raman spectra, for the perfect hexagonal graphite crystal is characterized by a sharp intense peak at 1575 cm^{-1}, called G-band (graphite band).[45] The G vibrational mode has an E_{2g} symmetry and corresponds to the in-plane bond stretching motion of pairs of C-sp^2 atoms. When a material is constituted by a random carbon structure, the Raman spectrum consists of two features: G-band, usually around 1580–1600 cm^{-1} and D-band (disordered band), usually around 1350 cm^{-1}.[46] The D-mode corresponds to a breathing mode of A_{1g} symmetry, which is forbidden in perfect graphite and only becomes active in the presence of disorder associated with finite crystalline sizes.[46] Thus, the D-band is usually associated with sp^3 carbon defects in a graphene layer or in the graphitic lattice.[47,48] Although the D-band arises from aromatic rings, it only appears in the presence of local disorder.[49] An increase in disorder leads to a decrease in the number of the Csp^2 clusters and they become smaller and more distorted. The I(D)/I(G) intensity ratio has been used to evaluate carbon-cluster size. For small graphitic domains (small L_a (lateral size)), the intensity of the D-mode is proportional to the probability of finding a sixfold ring in the cluster, that is, to the cluster area. Thus, in PDC this ratio can be described according to the following equation[46]

$$\frac{I(\mathrm{D})}{I(\mathrm{G})} = C(\lambda)L_a^2 \quad (1)$$

The value of the coefficient C depends on the wavelength of the radiation used. According to Ferrari and Robertson,[46] the value of C associated with radiation of 514.5 nm from the laser used in this study is 0.0055 $Å^{-2}$.

The ceramic samples obtained in this study showed similar Raman spectra, independent of the polymeric precursor compositions, as illustrated in Fig. 8 for H1 and HNi1 ceramics obtained at different pyrolysis temperatures. These samples presented the two characteristic modes (D- and G-modes) for C_{free} dispersed phases. Ceramic samples obtained at 950 °C exhibited a large fluorescence background, mainly above 2000 cm^{-1}, characteristic of these amorphous materials,[9] with broader D-and G-peaks. It has been reported that the pronounced fluorescence phenomenon prevented the identification of the free carbon phase in C-rich SiCO ceramics up to 1400 °C.[7,16] According to these authors, this phenomenon may be associated with defects present in the samples and radical formation during the polymer-to-glass transformation.

An increase in the pyrolysis temperature promoted a decrease in the fluorescence background. In addition, the valley between D-and G-bands became deeper, with smaller full width half-maxima (FWHM). At 1500 °C, the ceramic samples exhibited very distinct D- and G-bands, characterized by rather narrow peaks, which suggests that an ordering process occurred within the C_{free} phase during annealing, for all samples.

In a graphite-like phase, the position of the G-peak is affected by the amount of sp^3-sites.[46,49] Thus, an increase of sp^3-site content induces a shift of the G-peak position towards lower vibrational frequencies. In addition, the peak width also depends on the free carbon microstructure. As described earlier, crystalline graphite shows a sharp G-mode, while the presence of defects results in a broadening of the D-peak.[49]

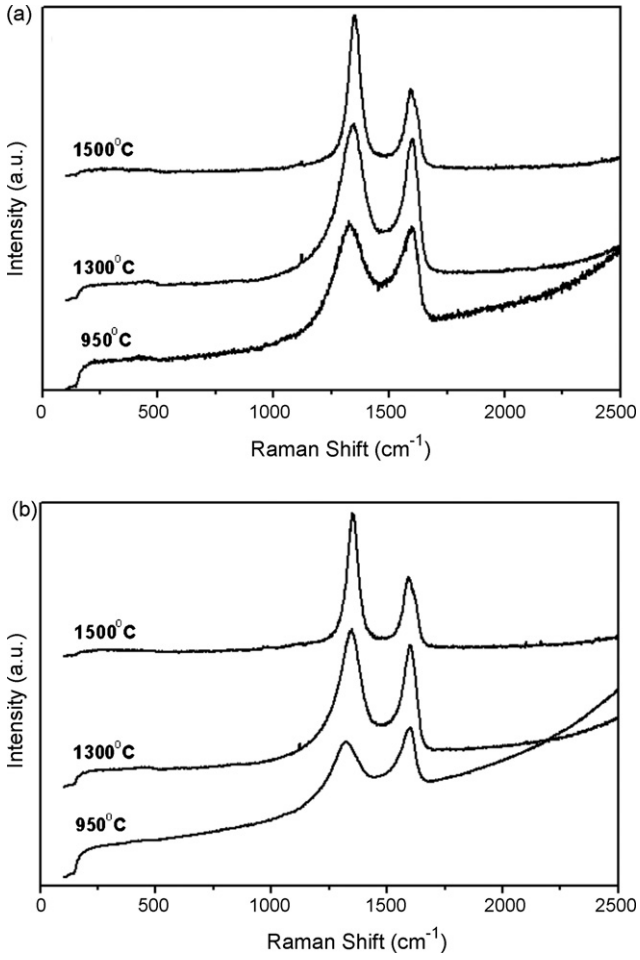

Fig. 8. Raman spectra for (a) H1 and (b) HNi1 ceramic samples obtained at different pyrolysis temperatures.

Based on these considerations, Lorentzian curve fitting[9,46] of the D- and G-bands was performed, in order to acquire useful parameters related to the evolution of the free carbon phase with increasing pyrolysis temperatures. In general, the heat-treatment promoted a shift of the G-peak to higher vibrational frequencies and a reduction of the FWHM of D- and G-bands, for all compositions, containing or not Ni (Table 4). These results suggest the occurrence of a reduction of defects within hexagonal carbon sheets has occurred with the increase of the pyrolysis temperature, due to the decrease of Csp^3-site amounts in these ceramics. Consequently, an increase of I(D)/I(G) intensity ratios was observed for all samples. This behavior is in agreement with data reported in literature, which predict that lower Csp^3-site total amounts give higher I(D)/I(G) ratios.[48] According to Eq. (1), the graphitic carbon domain size increased with the annealing temperature, varying from 1.3 to 1.8 nm for both systems. The graphitization process, identified by the separation between the D- and G-peaks, as well as the reduction of defects within the graphitic carbon phase, were also observed in SiCN ceramics, with an increase in the pyrolysis temperature, as described by Gregori et al.[49] However, Kleebe et al.[9] showed that the pyrolysis temperature did not affect the carbon domain size inside SiCO ceramics derived from a similar polymeric precur-

Table 4
Raman data for positions of D- and G-bands, half-height width of D and G-bands ($\Delta\nu_D$ and $\Delta\nu_G$) and $I(D)/I(G)$ ratio for all ceramic specimens with and without Ni at different pyrolysis temperatures

Samples	Temperature (°C)	D (cm^{-1})	G (cm^{-1})	$\Delta\nu_D$ (cm^{-1})	$\Delta\nu_G$ (cm^{-1})	$I(D)/I(G)$
	950	1338	1574	209	169	1.13
H1	1300	1341	1591	143	84	1.12
	1500	1350	1596	59	69	1.89
	950	1337	1575	235	130	1.05
H2	1300	1349	1596	63	65	1.80
	1500	1347	1588	88	74	1.42
	950	1328	1596	159	60	1.01
H3	1300	1351	1598	63	66	1.77
	1500	1346	1594	65	68	1.51
	950	1333	1590	230	71	1.43
HNi1	1300	1342	1595	131	69	1.21
	1500	1352	1596	56	66	1.82
	950	1339	1562	231	198	1.01
HNi2	1300	1347	1589	65	69	1.41
	1500	1340	1595	54	60	1.38
	950	1338	1571	214	170	0.99
HNi3	1300	1335	1596	176	75	1.13
	1500	1346	1587	58	64	1.38

sor, prepared from DVB (60 wt%). According to these authors, the formation of larger carbon domains is associated to diffusion and nucleation phenomena in addition to carbon–carbon bond rearrangements.

The β-SiC phase, which can be characterized by the presence of peaks at ~920, 830 and 431 cm^{-1}, [43,50] was not observed in the Raman spectra, in spite of it being clearly identified by XRD patterns. This is due to the lower Raman scattering efficiency for SiC, about 1/10 of the efficiency observed for graphitic carbon.[43,44] However, a very weak peak appeared at ~450 cm^{-1} in some samples.

Ceramic specimens were submitted to the nitrogen adsorption technique in order to characterize the micro- and mesopores in these materials as well as the specific surface area. Specific data extracted from isotherms such as specific surface area (SSA), mesopore and micropore volumes and average pore size are shown in Table 5. The increase in the pyrolysis temperature and variation in the polymeric precursor compositions promoted

Table 5
Specific surface area (SSA), mesopore and micropore volumes and average pore size for the ceramic specimens with and without Ni at different pyrolysis temperatures

Samples	Temperature (°C)	SSA (m^2/g)	Mesopore volume (10^{-3} cm^3/g)[a]	Micropore volume (10^{-3} cm^3/g)[b]	Average pore size (nm)
	950	–	–	–	–
H1	1300	–	–	–	–
	1500	3.1	2.8	0.8	3.9
	950	1.0	–	–	–
H2	1300	1.5	0.3	0.01	1.2
	1500	1.5	0.7	0.5	3.1
	950	1.2	–	–	4.2
H3	1300	2.7	–	–	1.9
	1500	0.8	0.9	0.07	4.7
	950	1.1	2.0	0.1	7.4
HNi1	1300	0.1	–	–	6.9
	1500	0.5	0.7	0.01	6.8
	950	0.7	–	–	8.3
HNi2	1300	3.6	3.2	0.07	4.5
	1500	188.4	305.8	6.8	6.2
	950	1.4	2.5	0.08	7.2
HNi3	1300	5.9	8.0	0.7	5.6
	1500	62.6	95.4	2.2	6.2

[a] As obtained from the BJH mesopore distribution using the desorption data of the isotherm.
[b] Calculated from *t*-plot analysis. Mesopore range = 2–50 nm. Micropore range <2 nm.

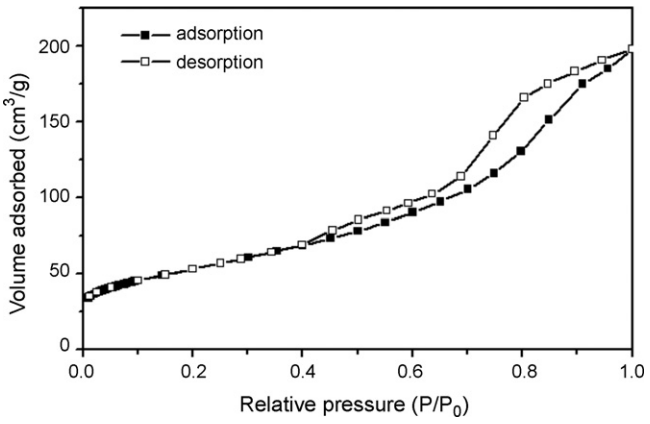

Fig. 9. Nitrogen adsorption–desorption isotherm for HNi2 obtained at 1500 °C.

few changes in the texture of the ceramics obtained without Ni. The profile of curves for these ceramics (not shown) was typical of non-porous materials, since the adsorbed gas volume remained practically constant throughout the pressure range. According to this behavior, these ceramics were truly dense materials showing negligible SSA values. In the Ni-containing ceramics, HNi1, revealed the same behavior as that the observed for the ceramics without Ni. However, the pyrolysis temperature was a determining factor to generate porosity, particularly when they were heated at 1500 °C, for HNi2 and HNi3. These samples presented SSA of 188.4 and 62.6 m^2/g, respectively, with an adsorption–desorption isotherm typical of mesoporous materials (Fig. 9).[26] In general, for both these ceramics the pore volume increased with the increase of the pyrolysis temperature, beyond of the extremely low values, while the average pore size did not show the same tendency. By comparing the data of ceramics with and without Ni, we can clearly state that the Ni-containing ceramics developed more porosity and larger pore sizes than the corresponding ceramics without Ni.

4. Conclusions

In the present study, PMS/DVB hybrid polymeric networks with different compositions were easily prepared by a hydrosilylation reaction, in the presence or not of NiAc. The influence of NiAc on the properties of the final ceramic products obtained at different pyrolysis temperatures was evaluated.

The increase of the pyrolysis temperature from 950 to 1500 °C resulted in continuous transformations of silicon sites until achieving segregation of the thermodynamically stable SiO_2 and SiC phases, in addition to a graphitic carbon phase. With respect to the C_{free} phase dispersed in the ceramic matrix, the graphitization process led to the reduction of defects within carbon sheets for the ceramic specimens, as demonstrated by Raman spectroscopy. In general, ceramics without Ni did not show porosity, independent of the pyrolysis temperature or polymeric precursor composition. However, the HNi2 and HNi3 samples obtained at 1500 °C revealed typical behaviors of mesoporous materials.

The ceramic materials obtained at 950 °C presented amorphous characters to X-ray diffraction. A crystalline β-SiC phase was generated when the ceramics were obtained at 1300 and 1500 °C. In addition to this phase, the presence of Ni induced the formation of other crystalline phases such as cristobalite silica, graphitic carbon, metallic nickel, NiO and Ni_2Si. The Ni-containing ceramics were denser than those without Ni as a consequence of these additional crystalline phases as well as larger SiC crystal sizes.

Acknowledgements

We gratefully acknowledge the financial support from FAPESP (Processes 05/58460-0 and 03/09926-1) and CNPq (Proc. 305916/2006-8). The authors also thank the Laboratório de Materiais, Prof. A. Lago, for Raman measurements and Prof. Dr. Carol H. Collins for English revision.

References

1. Julbe, A., Larbot, A., Guizard, C. and Cot, L., Characterization of silicon oxycarbide species. *Eur. J. Solid State Inorg. Chem.*, 1989, **26**, 101–110.
2. Renlund, G. M., Prochazka, S. and Doremus, R. H., Silicon oxycarbide glasses. Part II. Structure and properties. *J. Mater. Res.*, 1991, **6**, 2723–2734.
3. Breval, E., Hammond, M. and Pantano, C. G., Nanostructural characterization of silicon oxycarbide glasses and glass-ceramics. *J. Am. Ceram. Soc.*, 1994, **77**, 3012–3018.
4. Radovanovic, E., Gozzi, M. F., Gonçalves, M. C. and Yoshida, I. V. P., Silicon oxycarbide glasses from silicone networks. *J. Non-Cryst. Solids*, 1999, **248**, 37–48.
5. Wei, Q., Pippel, E., Woltersdorf, J., Scheffler, M. and Greil, P., Interfacial SiC formation in polysiloxane-derived Si–O–C ceramics. *Mater. Chem. Phys.*, 2002, **73**, 281–289.
6. Schiavon, M. A., Redondo, S. U. A., Pina, S. R. O. and Yoshida, I. V. P., Investigation on kinetics of thermal decomposition in polysiloxane networks used as precursors of silicon oxycarbide glasses. *J. Non-Cryst. Solids*, 2002, **304**, 92–100.
7. Bréquel, H., Parmentier, J., Walter, S., Badheka, R., Trimmel, G., Masse, S. *et al.*, Systematic structural characterization of the high-temperature behavior of nearly stoichiometric silicon oxycarbide glasses. *Chem. Mater.*, 2004, **16**, 2585–2598.
8. Berger, A., Pippel, E., Woltersdorf, J., Scheffler, M., Cromme, P. and Greil, P., Nanoprocesses in polymer-derived Si–O–C ceramics: electronmicroscopic observations and reaction kinetics. *Phys. Status Solidi (A)*, 2005, **202**, 2277–2286.
9. Kleebe, H.-J., Gregori, G., Babonneau, F., Blum, Y. D., MacQueen, D. B. and Masse, S., Evolution of C-rich SiOC ceramics. Part I. Characterization by integral spectroscopic techniques: solid-state NMR and Raman spectroscopy. *Int. J. Mater. Res.*, 2006, **97**, 699–709.
10. Schiavon, M. A., Radovanovic, E. and Yoshida, I. V. P., Microstructural characterization of monolithic ceramic matrix composites from polysiloxane and SiC powder. *Powder Technol.*, 2002, **123**, 232–241.
11. Kleebe, H.-J., Turquat, C. and Sorarù, G. D., Phase-separation in an SiCO glass studied by transmission electron microscopy and electron energy-loss spectroscopy. *J. Am. Ceram. Soc.*, 2001, **84**, 1073–1080.
12. Gregori, G., Kleebe, H. J., Blum, Y. D. and Babonneau, F., Evolution of C-rich SiOC ceramics. Part II. Characterization by high lateral resolution techniques: electron energy-loss spectroscopy, high-resolution TEM and energy-filtered TEM. *Int. J. Mater. Res.*, 2006, **97**, 710–720.
13. Turquat, C., Kleebe, H.-J., Gregori, G., Walter, S. and Sorarù, G. D., Transmission electron microscopy and electron energy-loss spectroscopy study of nonstoichiometric silicon-carbon-oxygen glasses. *J. Am. Ceram. Soc.*, 2001, **84**, 2189–2196.

14. Schiavon, M. A., Sorarù, G. D. and Yoshida, I. V. P., Poly(borosilazanes) as precursors of Si–B–C–N glasses: synthesis and high temperature properties. *J. Non-Cryst. Solids*, 2004, **348**, 156–161.
15. Liebau, V., Hauser, R. and Riedel, R., Amorphous SiBCO ceramics derived from novel polymeric precursors. *C.R. Chim.*, 2004, **7**, 463–469.
16. Alonso, R. P., Mariotto, G., Gervais, C., Babonneau, F. and Sorarù, G. D., New insights on the high-temperature nanostructure evolution of SiOC and B-doped SiBOC polymer-derived glasses. *Chem. Mater.*, 2007, **19**, 5694–5702.
17. Schiavon, M. A., Gervais, C., Babonneau, F. and Sorarù, G. D., Crystallization behavior of novel silicon boron oxycarbide glasses. *J. Am. Ceram. Soc.*, 2004, **87**, 203–208.
18. Scheffler, M., Greil, P., Berger, A., Pippel, E. and Woltersdorf, J., Nickel-catalysed in situ formation of carbon nanotubes and turbostratic carbon in polymer-derived ceramics. *Mater. Chem. Phys.*, 2004, **84**, 131–139.
19. Haberecht, J., Krumeich, F., Stalder, M. and Nesper, R., Carbon nanostructures on high-temperature ceramics—a novel composite material and its functionalization. *Catal. Today*, 2005, **102/103**, 40–44.
20. Deng, S. Z., Li, Z. B., Wang, W. L., Xu, N. S., Zhou, J., Zheng, X. G. *et al.*, Field emission study of SiC nanowires/nanorods directly grown on SiC ceramic substrate. *Appl. Phys. Lett.*, 2006, **89**, 023118–023118-3.
21. Cheng, J., Zhang, X. and Ye, Y., Synthesis of nickel nanoparticles and carbon encapsulated nickel nanoparticles supported on carbon nanotubes. *J. Solid State Chem.*, 2006, **179**, 91–95.
22. Pinho, R. O., Radovanovic, E., Torriani, I. L. and Yoshida, I. V. P., Hybrid materials derived from divinylbenzene and cyclic siloxane. *Eur. Polym. J.*, 2004, **40**, 615–622.
23. Cullity, B. D., *Elements of X-ray Diffraction*. Addison-Wesley, Reading, 1978, pp. 284–285.
24. Azároff, L. V., *Elements of X-ray Crystallography*. McGraw-Hill, New York, 1968, pp. 549–552.
25. Borda, P. P. and Legzdins, P., Determination of carbon content in carbides by an elemental analyzer. *Anal. Chem.*, 1980, **52**, 1777–1778.
26. Webb, P. A. and Orr, C., *Analytical Methods in Fine Particle Technology*. Micromeritics Instrument Corp., Norcross, USA, 1997, pp. 53–153.
27. Brunauer, S., Emmett, P. H. and Teller, E., Adsorption of gases in multimolecular layers. *J. Am. Chem. Soc.*, 1938, **60**, 309–319.
28. Barrett, E. P., Joyner, L. G. and Halenda, P. P., The determination of pore volume and area distributions in porous substances. I. Computations from nitrogen isotherms. *J. Am. Chem. Soc.*, 1951, **73**, 373–380.
29. Camino, G., Lomakin, S. M. and Lazzari, M., Polydimethylsiloxane thermal degradation. Part I. Kinetic aspects. *Polymer*, 2001, **42**, 2395–2402.
30. Camino, G., Lomakin, S. M. and Lageard, M., Thermal polydimethylsiloxane degradation. Part 2. The degradation mechanisms. *Polymer*, 2002, **43**, 2011–2015.
31. Michalczyk, M. J., Farneth, W. E. and Vega, A. J., High-temperature stabilization of cross-linked siloxanes glasses. *Chem. Mater.*, 1993, **5**, 1687–1689.
32. Blum, Y. D., MacQueen, D. B. and Kleebe, H.-J., Synthesis and characterization of carbon-enriched silicon oxycarbides. *J. Eur. Ceram. Soc.*, 2005, **25**, 143–149.
33. Bellamy, L. J., *The Infra-red Spectra of Complex Molecules*. John Wiley & Sons, London, 1958, pp. 65, 340.
34. Li, F., Wen, G. and Song, L., Growth of nanowires from annealing SiBONC nanopowders. *J. Cryst. Growth*, 2006, **290**, 466–472.
35. Yang, Z. X., Zhou, W. M., Zhu, F. and Zhang, Y. F., SiC/SiO_2 core–shell nanocables formed on the carbon fiber felt. *Mater. Chem. Phys.*, 2006, **96**, 439–441.
36. Graetsch, H., Gies, H. and Topalović, I., NMR, XRD and IR study on microcrystalline opals. *Phys. Chem. Miner.*, 1994, **21**, 166–175.
37. Graetsch, H., Mosset, A. and Gies, H., XRD and ^{29}Si MAS-NMR study on some non-crystalline silica minerals. *J. Non-Cryst. Solids*, 1990, **119**, 173–180.
38. Bois, L., Maquet, J. and Babonneau, F., Structural characterization of sol–gel derived oxycarbide glasses. 2. Study of the thermal stability of the silicon oxycarbide phase. *Chem. Mater.*, 1995, **7**, 975–981.
39. Liu, X., Yang, Y., Ji, W., Liu, H., Zhang, C. and Xu, B., Controllable growth of nanostructured carbon from coal tar pitch by chemical vapor deposition. *Mater. Chem. Phys.*, 2007, **104**, 320–326.
40. Zhang, Z., Zhao, Y. and Zhu, M., NiO films consisting of vertically aligned cone-shaped NiO rods. *Appl. Phys. Lett.*, 2006, **88**, 033101-1–033101-3.
41. Kim, Y.-W., Kim, S.-H., Kim, H.-D. and Park, C. B., Processing of closed-cell silicon oxycarbide foams from a preceramic polymer. *J. Mater. Sci.*, 2004, **39**, 5647–5652.
42. Rouxel, T., Massouras, G. and Sorarù, G. D., High temperature behavior of a gel-derived SiOC glass: elasticity and viscosity. *J. Sol–Gel Sci. Technol.*, 1999, **14**, 87–94.
43. Gozzi, M. F. and Yoshida, I. V. P., Structural evolution of a poly(methylsilane)/tetra-allylsilane mixture into silicon carbide. *Eur. Polym. J.*, 1997, **33**, 1301–1306.
44. Li, X. and Edirisinghe, M. J., Structural evaluation of polysilane-derived products: from amorphous to thermodynamically stable phases. *Philos. Mag.*, 2004, **84**, 647–671.
45. Tuinstra, F. and Koenig, J. L., Raman spectrum of graphite. *J. Chem. Phys.*, 1970, **53**, 1126–1130.
46. Ferrari, A. C. and Robertson, J., Interpretation of Raman spectra of disordered and amorphous carbon. *Phys. Rev. B*, 2000, **61**, 14095–14107.
47. Gualandris, V., Bahloul, D. H. and Babonneau, F., Structural investigation of the first stages of pyrolysis of Si–C–O preceramic polymers containing Si–H bonds. *J. Sol–Gel Sci. Technol.*, 1999, **14**, 39–48.
48. Kolar, F., Machovic, V., Svítilová, J. and Brecká, L., Structural characterization and thermal oxidation resistance of silicon oxycarbides produced by polysiloxane pyrolysis. *Mater. Chem. Phys.*, 2004, **86**, 88–98.
49. Gregori, G., Kleebe, H.-J., Brequel, H., Enzo, S. and Ziegler, G., Microstructure evolution of precursors-derived SiCN ceramics upon thermal treatment between 1000 and 1400 °C. *J. Non-Cryst. Solids*, 2005, **351**, 1393–1402.
50. Trassl, S., Motz, G., Rössler, E. and Ziegler, G., Characterization of the free-carbon phase in precursor-derived SiCN ceramics. *J. Non-Cryst. Solids*, 2001, **293–295**, 261–267.